

Time Delay between Relativistic Images as a probe of Cosmic Censorship

Satyabrata Sahu^{*,1}, Mandar Patil^{†,1,2} and D. Narasimha[‡], Pankaj S. Joshi^{§1}

¹*Tata Institute of Fundamental Research*

Homi Bhabha Road, Mumbai 400005, India

²*Inter-University Centre for Astronomy and Astrophysics*

Ganeshkhind, Pune 411 007, India

Abstract

We study the time delay between successive relativistic images in gravitational lensing as a possible discriminator between various collapse end states and hence as a probe of cosmic censorship. Specifically we consider both black hole and naked singularity spacetimes admitting photon spheres where infinite number of relativistic Einstein Rings can be formed at almost same radius and naked singularity spacetimes without photon sphere where multiple relativistic Einstein Rings can form almost up to the center of the lens. The metrics we have considered to sample these scenarios are the Schwarzschild black hole, Janis-Newman-Winicour (naked singularity with photon sphere), Joshi-Malfarina-Narayan, & Tolman-VI (naked singularities without photon sphere) which are a fair sample of the theoretical possibilities. We show that the differential time delay between the relativistic images for naked singularities without photon sphere progressively decreases for the models we study as opposed to that for black holes and naked singularities with photon sphere, where it is known to be roughly constant. This characteristic difference in time delay between successive images for these two cases can be potentially exploited for a source with known intrinsic variability to discriminate between these scenarios even when the images are not spatially resolved.

PACS numbers: 95.30.Sf, 04.20.Dw, 04.70.Bw, 98.62.Sb

* Electronic address: satyabrata@tifr.res.in

† Electronic address: mandar@iucaa.ernet.in

‡ Electronic address: dna@tifr.res.in

§ Electronic address: psj@tifr.res.in

I. INTRODUCTION

Gravitational lensing is a powerful astrophysical as well as cosmological probe to study the lens object, source as well as the background geometry and it indirectly serves as a probe of gravitational physics. Gravitational lensing can help us to detect or infer the existence of exotic objects in the universe. When the lens is a very compact object (e.g. a black hole or the alternative end states of collapse), light rays can probe the strong gravitational field produced by them and gravitational lensing becomes a powerful probe of physics in strong gravity regime. If the lens is compact enough and light rays can explore spacetime close enough to it, then the deflection angle can become more than 2π [1, 2]. Moreover propagation of light in the vicinity of black holes or compact enough objects leads to interesting signatures in apparent position and flux of images for sources near (and orbiting) such objects [3–5]. These signatures constitute important strong field tests of General Relativity. For faraway sources lensed by a compact object, when deflection angle exceeds 2π , two sequences of images are formed on different sides of the lens due to photons which undergo one or more turns around the lens (the deflection angles are close to $2\pi, 4\pi$ etc.) in addition to two (far-field) images of the source formed due to photons which undergo small deflection (the so-called primary and secondary images). These additional images are called relativistic images, the phenomenon is called relativistic lensing [6, 7].

One of the exciting questions that the phenomenon of relativistic lensing can help us address is Cosmic Censorship conjecture [8] and the related questions of end state of gravitational collapse and final fate of massive stars [9]. Cosmic censorship conjecture, viz. the proposal that naked singularities do not occur in nature, still remains an open issue. On the other hand it has been shown that both black holes and naked singularities can form in gravitational collapse of a matter cloud (obeying certain energy conditions for physical reasonability) starting from a regular initial data [10–12]. For example, while homogeneous dust collapse always results in a black hole, inhomogeneous dust collapse with decreasing density profile away from center can result in both black holes and naked singularities as endstates [10]. Similar conclusion follows from study of more complex scenarios with inclusion of pressure. There remains still the question of whether one needs finely tuned initial data to form naked singularities. Strictly restricting to spherically symmetric collapse, one does have a concrete realization of naked singularity formation without need of fine tuning initial data. The general relativistic Larson-Penston solution, which is obtained without fine-tuning in spherically symmetric collapse of perfect fluid with a soft equation of state ($p = k\rho$ for $0 < k \leq 0.03$) [13] is stable against spherical linear perturbations and describes the

formation of naked singularity for $0 < k < 0.0105$, ie for extremely soft equation of state [14, 15]. Furthermore it was shown in [16] that for spherically symmetric gravitational collapse of a general Type I matter field, when the effects of small pressure perturbations in an otherwise pressure-free collapse scenario is taken into account, both black holes and naked singularities are generic (for suitable definition of genericity) outcomes of a complete collapse. Non-spherical collapse has also been studied (see [11] and references therein); but it is fair to say that a lot needs to be done before a conclusion can be arrived at for fine tuning issues in non-spherical collapse scenarios. However one can adopt the point of view alluded to in [11] that ‘if cosmic censorship is to hold as a basic principle of nature, it better holds in spherical class too’ and consider it worthwhile to investigate astrophysical implications of naked singularities. We must, all the same, mention that the examples studied here are toy models and we hope that it captures qualitatively the basic physics so as to guide future explorations.

A lot of black hole candidates (compact,dark, heavy objects) have been discovered observationally and most likely they are indeed black holes [17]. However in the absence of concrete theoretical reasons to rule out naked singularity and in the face of our relative ignorance of behavior of matter in extremely high density configuration which is reached towards the end of the gravitational collapse of a massive stars, one can take a phenomenological approach, ie, compute the signatures of the naked singularities and confront them with observations. Gravitational lensing signatures of naked singularity will then be very useful in this regard. With this philosophy, Virbhadra,Narasimha and Chitre [18] and later Virbhadra and Ellis [7] and Virbhadra and Keeton [19] have studied and compared gravitational lensing by Schwarzschild black holes and by the Janis, Newman, Winicour naked singularities (JNW solution). Gravitational lensing by rotating version of JNW naked singularity has been studied in [20]. Extending the same line of work, we have recently studied a class of naked singularity solutions obtained as the end state of certain dynamical collapse scenarios for a fluid with only tangential pressure [21]. In this work, we take this program further to study a generalization of this model ,ie., an analogous scenario for a fluid with non-zero radial as well as tangential pressure, to examine if the earlier conclusions obtained for the tangential pressure case also generalize qualitatively. Furthermore we focus on role of time delay in relativistic lensing from this perspective by studying time delay between relativistic Einstein Rings for all the above mentioned solutions. It is worth noting here that apart from lensing, accretion disk properties has been also explored recently as a probe of cosmic censorship [22, 23].

As we have discussed earlier in the strong gravity regime, like a black hole, the bending angle could be more than 2π and multiple relativistic images might be formed. In the case of formation

of multiple images, the light-travel-time along light paths corresponding to different images is different. Therefore, if the background source in the lens system were to be variable, this variability will not appear simultaneously in the images. So, intrinsic luminosity variations of the source manifests in the images as a relative temporal phase which is expected to depend on the lens geometry and lensing configuration. The time lag for appearance of the intrinsic variability between the multiple images is called the time delay. Time delay has a privileged status among lensing observable in the sense that it is the only dimensional observable and as such only observable sensitive to overall scaling of all the distance scales in the problem. The observed configuration in the sky imposes dimensionless constraints only, but time delay introduces a physical scale in the system. That makes it a useful probe of mass of the lens as well as distances between lens and observer etc. In cosmological contexts, it has been argued to be a probe of the Hubble parameter [24, 25]. In the conventional post-Newtonian approximation, the difference in the light travel time can be decomposed into a geometrical component due to difference in the path length and a potential component due to the different Newtonian gravitational potential felt by the photon. Time delay between far field images is a probe of the so-called ‘effective distance’ of the system and can be a probe of cosmological parameters [26]. Time delay between relativistic images for black hole has been suggested as a distance estimator [27]. In this paper we focus on time delay as a discriminator between black hole and naked singularity. For this we study Schwarzschild black hole, JNW naked singularity, JMN solution and Tolman-VI solution. The last two solutions have been shown to be obtainable as collapse end states [23, 28]. Time delay between relativistic images have previously been studied for Schwarzschild black hole in [6] and in general for spacetimes with photon spheres in [27] (which includes black holes and Weakly Naked Singularities, as we will see later). The present study complements these by computing time delay between relativistic images for Strongly Naked Singularities, ie., naked singularities not covered by photon sphere. To give a feel for the numbers, we consider both the case of super massive objects at galactic centers (most likely super massive black holes [29]) as well as $100M_{\odot}$ objects in our galaxy.

This paper is organized as follows. In section II we briefly discuss lensing formalism and in section III we introduce the spacetimes we are going to study. In section IV we discuss the photon spheres in these spacetimes and in section V we discuss possibility of relativistic lensing and the basic features of relativistic images. Then in section VI we discuss Einstein Rings and section VII we present a discussion of time delay between the Einstein Rings for various scenarios under consideration and highlight the main differences between black holes and strongly naked singularities. Finally we conclude with a discussion of main results in VIII. We work in units of

$c = 1$ and $G = 1$ through out the paper.

II. LENSING FORMALISM

In this section we briefly review the gravitational lensing formalism [7, 18]. We consider a spherically symmetric, static and asymptotically flat spacetime to be thought of as gravitational lens. Source and observer are assumed to be sufficiently away from the central region. There are two important parts to the lensing formalism. First one is the lens equation which relates image location to the source location given the deflection angle and this is essentially a geometrical relation written down taking advantage of asymptotic flatness. For a very nice discussion on various lens equations in literature, refer to [30]. The second part is the calculation of deflection angle which is computed by integrating the null geodesics. It is through this deflection angle that General Relativity enters into picture for calculation of lensing observables such as image position and magnification.

We use the Virbhadra-Ellis lens equation [7] which is given by the following expression.

$$\tan \beta = \tan \theta - \alpha \quad (1)$$

where

$$\alpha = \frac{D_{ds}}{D_s} [\tan \theta + \tan (\hat{\alpha} - \theta)] \quad (2)$$

where θ, β denote the image location and source location respectively (see Fig 1). We also have $\sin \theta = \frac{J}{D_d}$ where J is the impact parameter.

The general form of the metric is given by

$$ds^2 = -g(r)dt^2 + \frac{1}{f(r)}dr^2 + h(r)r^2d\Omega^2 \quad (3)$$

The total deflection suffered by the light ray as it travels from source to observer is given by

$$\hat{\alpha}(r_0) = 2 \int_{r_0}^{\infty} \left(\frac{1}{f(r)h(r)} \right)^{1/2} \left[\left(\frac{r}{r_0} \right)^2 \frac{h(r)}{h(r_0)} \frac{g(r_0)}{g(r)} - 1 \right]^{-1/2} \frac{dr}{r} - \pi, \quad (4)$$

where r_0 is the distance of closest approach. The relation between impact parameter and the distance of closest approach is given by $J = r_0 \sqrt{\frac{h(r_0)}{g(r_0)}}$.

Image location θ is obtained by solving the lens equation for the fixed value of source location β . The magnification is defined as

$$\mu \equiv \left(\frac{\sin \beta}{\sin \theta} \frac{d\beta}{d\theta} \right)^{-1}. \quad (5)$$

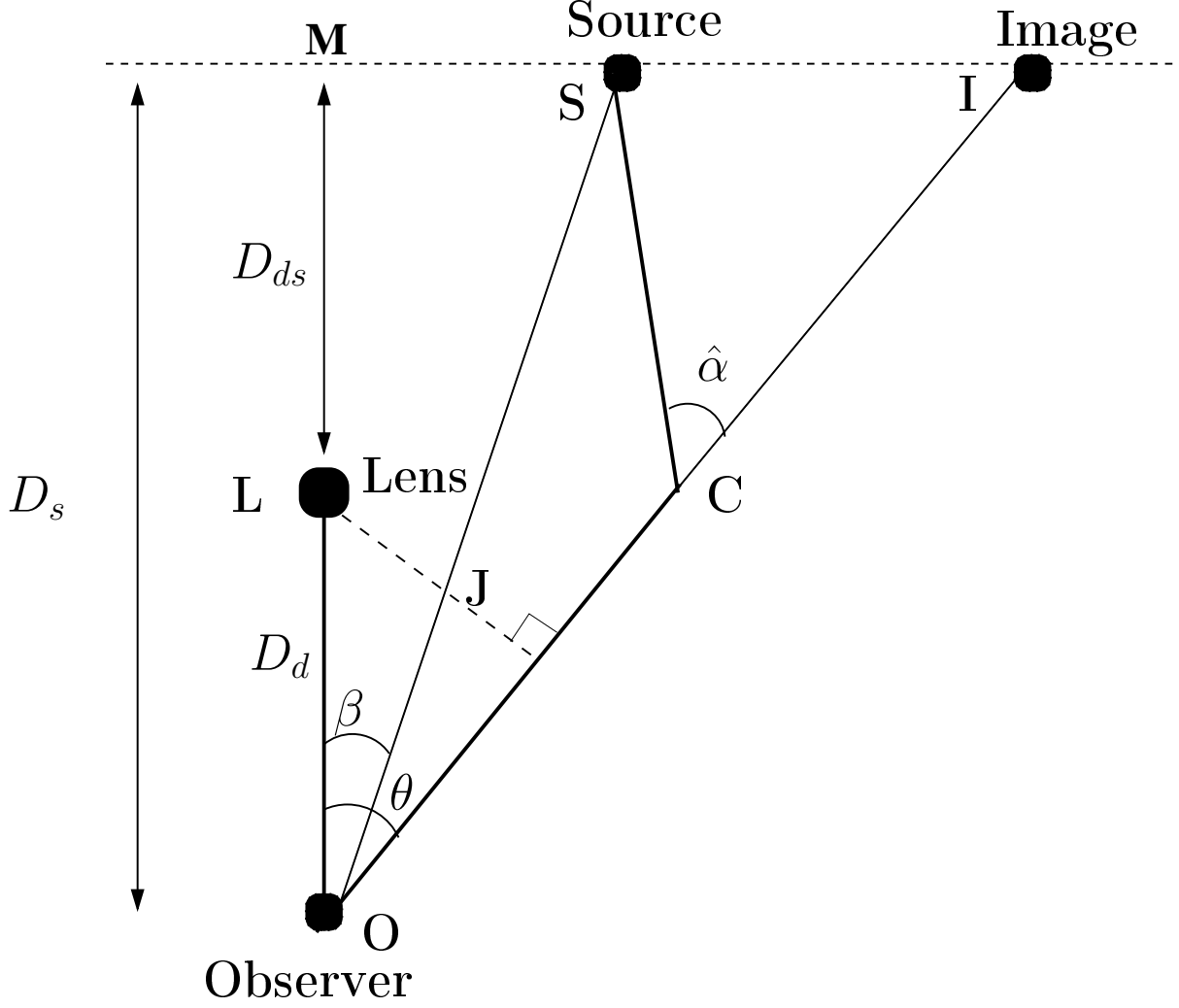


FIG. 1: *Len Diagram*: Positions of the source, lens, observer and the image are given by S , L , O and I . The distances between lens-source, lens-observer and source-observer are given by D_{ds} , D_d and D_s . The angular location of the source and the image with respect to optic axis are given by β and θ . The impact parameter is given by J .

which can be broken down into the tangential and radial magnification in the following way.

$$\mu_t \equiv \left(\frac{\sin \beta}{\sin \theta} \right)^{-1}, \quad \mu_r \equiv \left(\frac{d\beta}{d\theta} \right)^{-1} \quad (6)$$

Singularities of the tangential and radial magnification give tangential and radial critical curves and caustics. We discuss time delay separately in section VII.

III. SPACETIMES UNDER CONSIDERATION

We will be considering static spherically symmetric spacetimes for simplicity. Under these assumptions the simplest black hole solution is the Schwarzschild solution which is given by

$$ds^2 = - \left(1 - \frac{2M}{r}\right) dt^2 + \left(1 - \frac{2M}{r}\right)^{-1} dr^2 + r^2 d\Omega^2 \quad (7)$$

where M is the Schwarzschild mass. A naked singularity solutions which has been studied in literature is the JNW solution [7, 18]. It is a solution of Einstein equations with a minimally coupled massless canonical scalar field and is parametrized by two parameters, mass M and scalar charge q . The solution can be written as

$$ds^2 = - \left(1 - \frac{b}{r}\right)^\nu dt^2 + \left(1 - \frac{b}{r}\right)^{-\nu} dr^2 + \left(1 - \frac{b}{r}\right)^{1-\nu} r^2 d\Omega^2 \quad (8)$$

where $b = 2\sqrt{M^2 + q^2}$ and $\nu = \frac{2M}{b}$.

Because of absence of analogues of black hole uniqueness theorems for naked singularities, it becomes necessary to study other possible naked singularity solutions in order to properly gauge the prospects of any observational probe (like gravitational lensing) for shedding light on cosmic censorship question. Below we describe two naked singularity solutions which, unlike the JNW solution described above, have been shown to be obtainable as collapse end states [23, 28]. Admittedly these too are toy models, but study of these solutions can be thought of as a step in the direction of study of more realistic models where by realistic we mean a naked singularity solution generated by a well motivated source, possibly taking into account deviations from spherical symmetry in the form of higher multipoles (which becomes important because of absence of analogues of black hole uniqueness theorems for naked singularities), and shown to be stable under linear (and non-linear) perturbations etc. Unfortunately such analytic solutions are hard to find or construct. One can then investigate various toy model scenarios to gather some idea of what is to be expected in a ‘realistic’ scenario. This is expected to provide valuable insights as far as qualitative features are concerned. JNW solution mentioned above, which is well studied in literature from lensing perspective [7, 18] is one such toy model as are the two solutions we describe below. One can hope that these examples capture most of the essential features of a realistic model at least for spherically symmetric situation and observational features would generalize qualitatively.

One of the examples is the JMN naked singularity which was shown to be obtainable as the end state of dynamical collapse from regular initial conditions for a fluid with zero radial pressure

but non-vanishing tangential pressure [28] and was studied in [21] from lensing perspective. The interior region in this spacetime is described by the metric

$$ds_e^2 = -(1 - M_0) \left(\frac{r}{R_b} \right)^{\frac{M_0}{1-M_0}} dt^2 + \frac{dr^2}{1 - M_0} + r^2 d\Omega^2. \quad (9)$$

The solution has a naked singularity at the center and matches to a Schwarzschild spacetime across the boundary $r = R_b$ with the Schwarzschild mass given by $M = \frac{M_0 R_b}{2}$. There are two parameters in the solution, M_0 which is a dimensionless parameter and, M is the Schwarzschild mass. We must have $0 < M_0 < 1$ for satisfying the condition that sound speed inside the cloud is always positive and less than speed of light [28]. As mentioned before, the radial pressure of the interior fluid is zero and the tangential pressure p_t is related to energy density ρ as

$$p_t = \frac{M_0}{4(1 - M_0)} \rho \quad (10)$$

Thus tangential pressure is linearly related to energy density. Both energy density and tangential pressure fall off as $1/r^2$. In addition to these, the fourth example that we consider in this paper is a static perfect fluid sphere solution given by Tolman [31] which also happens to be obtainable as collapse end state [23]. We note here that basic features of accretion disks in JMN and above Tolman solution was studied and contrasted with black hole case in [28] and [23] respectively. Below we describe the Tolman solution (henceforth to be referred to as Tolman-VI solution) briefly.

The metric in the interior is given by

$$ds_e^2 = -(Ar^{1-\lambda} - Br^{1+\lambda})^2 dt^2 + (2 - \lambda^2) dr^2 + r^2 d\Omega^2 \quad (11)$$

which has a central singularity and is matched to a Schwarzschild spacetime via C^2 matching. The number of parameters describing the solution as written above is 5 viz, A, B, λ (which characterize the fluid via its pressure and energy density) M the Schwarzschild mass and R_b , the boundary of the cloud which is the matching radius. However three matching conditions, viz, matching of g_{rr} , g_{tt} and pressure across the boundary, reduce the number of independent variables to 2 and we take λ and M as the independent variables. Then we have

$$R_b = \frac{2M(2 - \lambda^2)}{1 - \lambda^2} \quad (12)$$

$$A = \frac{(1 + \lambda)^2}{4\lambda\sqrt{2 - \lambda^2}} \left(\frac{2M(2 - \lambda^2)}{1 - \lambda^2} \right)^{\lambda-1} \quad (13)$$

$$B = \frac{(1 + \lambda)^2}{4\lambda\sqrt{2 - \lambda^2}} \left(\frac{1 - \lambda}{1 + \lambda} \right)^2 \left(\frac{2M(2 - \lambda^2)}{1 - \lambda^2} \right)^{-\lambda-1} \quad (14)$$

By imposing the condition that sound speed inside the cloud is always positive and less than speed of light ie $c_s < 1$ one gets a bound on physically admissible range of λ , viz, $\lambda \in (0, 1)$ [23]. The interior fluid has pressure p and energy density ρ related as

$$p = \frac{1}{1 - \lambda^2} \frac{(1 - \lambda)^2 - (1 + \lambda)^2 r^{2\lambda} (B/A)}{1 - r^{2\lambda} (B/A)} \rho \quad (15)$$

which upon using matching conditions becomes

$$p = \frac{(1 - \lambda)^2}{1 - \lambda^2} \frac{1 - \left(\frac{r}{R_b}\right)^{2\lambda}}{1 - \left(\frac{r}{R_b}\right)^{2\lambda} \left(\frac{1 - \lambda}{1 + \lambda}\right)^2} \rho \quad (16)$$

Both energy density and pressure fall off as $1/r^2$ near center and far off.

For convenience we introduce dimensionless variables (scaling all quantities by $2M$) $x \equiv \frac{r}{2M}$, $a \equiv \frac{A}{(2M)^{-1+\lambda}}$, $b \equiv \frac{B}{(2M)^{-1-\lambda}}$. The dimensionless boundary radius is then given by

$$x_b \equiv \frac{R_b}{2M} = \frac{2 - \lambda^2}{1 - \lambda^2} \quad (17)$$

which means that the compactness of the solution $\frac{2M}{R_b}$ is determined by λ alone. Similarly a and b are also determined by λ . For convenience again we define $\kappa \equiv \frac{b}{a}$. One then gets

$$a = \frac{(1 + \lambda)^2}{4\lambda\sqrt{2 - \lambda^2}} \left(\frac{2 - \lambda^2}{1 - \lambda^2}\right)^{\lambda-1} \quad (18)$$

$$\kappa = \left(\frac{1 - \lambda}{1 + \lambda}\right)^2 \left(\frac{1 - \lambda^2}{2 - \lambda^2}\right)^{2\lambda} \quad (19)$$

IV. PHOTON SPHERE

One important question for relativistic lensing is the presence/absence of photon sphere. The deflection angle diverges in the limit where distance of closest approach approaches the radius of photon sphere. In fact it diverges logarithmically as demonstrated by Bozza [32]. Photon sphere is a time-like hypersurface generated by circular closed null-geodesics in the spacetime. So it can be obtained by solving for $r = \text{constant}$ null-geodesics or in other words for the minima/maxima for effective potential for photons which as has already been mentioned is given by equation 20. Alternatively Photon sphere can also be defined as a time-like hypersurface $r = r_{ph}$ such that the deflection angle becomes infinity when the closest distance of approach r_0 tends to r_{ph} [7]. The equation of the photon sphere for metric given by 3 can be written as

$$\frac{g(r)'}{g(r)} = \frac{h(r)'}{h(r)} + \frac{2}{r} \quad (20)$$

where $'$ denotes derivative with respect to r . For a generalization of the concept of photon sphere to arbitrary spacetime see [33]. It can be argued that any spherically symmetric and static spacetime that has a horizon and is asymptotically flat for $r \rightarrow \infty$ must contain a photon sphere [34] and hence any black hole will always give rise to relativistic deflection and relativistic images. On the other hand a naked singularity may or may not have a photon sphere surrounding it and although a photon sphere guarantees relativistic images, one may or may not form relativistic images in the absence of photon sphere. Depending on whether or not the naked singularity is surrounded by a photon sphere Virbhadra and Ellis [7] classified the naked singularities as weakly naked singularity (WNS) and strongly naked singularity (SNS). The ones surrounded by photon sphere are called weakly naked (WNS) while those not surrounded by photon sphere are referred to as strongly naked (SNS). The spacetimes we study in this paper include examples of black holes, SNS and WNS giving rise to relativistic images. We wish to clarify here that this terminology should not be confused with classification of naked singularities into ‘strong curvature singularity’ and ‘weak curvature singularity’ on the basis of extendibility of spacetime through the singularity [10].

We also note here that for the definition presented in [7] it is in principle possible to have WNS with multiple photon spheres. For example one could have a stable photon sphere interior to the outer unstable photon sphere. In such cases one can have null geodesics coming from infinity, going inside the photon sphere and coming back to infinity as is easy to see from effective potential for photons in such spacetimes. Also there could be multiple photon sphere spacetimes [35]. For such cases lensing signature are expected to be different from single photon sphere and we briefly comment on this point in section V. The WNS spacetimes studied in this paper do not come in this category and always have a single photon sphere and the statements we make for WNS case henceforth shall consider such cases only.

For Schwarzschild geometry the equation of photon sphere is satisfied at $x = 3/2$ where $x = r/2M$. In any metric matched to Schwarzschild exterior (which is the case for both JMN and Tolman-VI metric that we are studying), the presence of photon sphere in Schwarzschild exterior depends on the dimensionless matching radius x_b . Clearly if and only if $x_b < 3/2$, the exterior photon sphere will be present. For JMN metric this condition translates to $M_0 > 2/3$. Also as was discussed in [21] the interior solution has no photon sphere when $M_0 \neq 3/2$. Thus JMN metric has a photon sphere in the Schwarzschild exterior if $M_0 > 2/3$ and no photon sphere otherwise.¹ On the other hand for Tolman-VI metric, using $\lambda \in (0, 1)$ and 17 one gets $R_b > 4M$

¹ We neglect the slightly unusual case $M_0 = 2/3$ for which there is (neutral) photon sphere at *every* radius inside

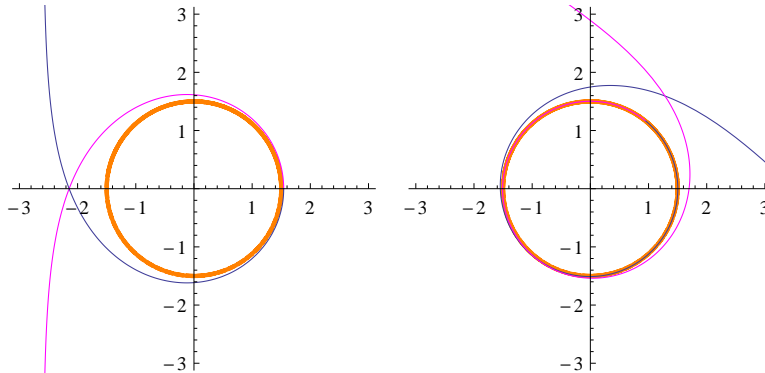


FIG. 2: Schematic photon trajectory for relativistic deflection in spacetime with photon sphere with both axes plotted in Schwarzschild units (photon sphere is given by the thick orange circle; in the two-loop case the second loop is virtually indistinguishable from the photon sphere)

which implies $x_b > 2 > 3/2$. So in no regime of parameter space for this geometry one can have a photon sphere in exterior Schwarzschild spacetime. The condition for existence of photon sphere inside the cloud reduces to $x^{2\lambda} = -\frac{a}{b}$ and owing to positivity of a and b there is no photon sphere in the interior geometry either. Thus there is no photon sphere in this geometry for *any* value of allowed parameter range. In JNW solution for low scalar charge $q/M \leq \sqrt{3}$ one has photon sphere and hence is an example of a weakly naked singularity [18]. In this paper we will not be concerned with the case $q/M > \sqrt{3}$ as we want to use JNW solution to illustrate the case of a Naked Singularity with photon sphere. JMN for $M_0 > 2/3$ is lensing signature-wise exactly identical to Schwarzschild as discussed in ref [21] and won't be considered here. Both JMN for $M_0 < 2/3$ and Tolman-VI serve as examples of strongly naked singularities, i.e., naked singularity without photon sphere.

In figure 2 we show schematically the photon trajectory for photons traveling in loops in spacetime with photon sphere. As one can see the successive loops are anchored on the photon sphere. In contrast we show the photon trajectory for photons traveling in loops in spacetime without photon sphere in figure 3. This picture will help in an intuitive understanding of the differences in time delay results we discuss later.

the cloud.

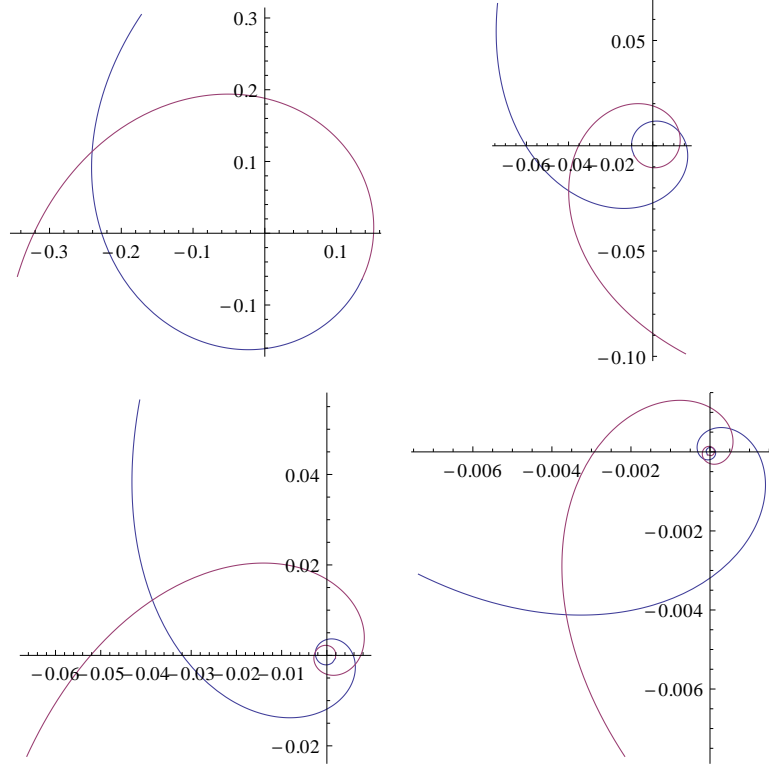


FIG. 3: Schematic photon trajectory for relativistic deflection in spacetime without photon sphere with both axes plotted in Schwarzschild units

V. RELATIVISTIC DEFLECTION AND IMAGES

Using formula 4 , the deflection angle in Schwarzschild in terms of dimensionless variables is given as

$$\hat{\alpha}(x_0) = 2 \int_{x_0}^{\infty} \left(\frac{1}{1 - \frac{1}{x}} \right)^{1/2} \left(\frac{x}{x_0} \right)^2 \left[\left(\frac{x}{x_0} \right)^2 \left(\frac{1 - \frac{1}{x_0}}{1 - \frac{1}{x}} \right) - 1 \right]^{-1/2} \frac{dx}{x} - \pi \quad (21)$$

and

$$\sin \theta = \frac{2M}{D_d} \frac{x_0}{\sqrt{1 - \frac{1}{x}}} \quad (22)$$

allows us to express deflection angle as a function of image location $\hat{\alpha}(\theta)$. For corresponding expressions in JMN refer to [21] and for JNW to [7]. For Tolman-VI we have for $x_0 < x_b$

$$\hat{\alpha}(x_0) = 2 \int_{x_0}^{x_b} (2 - \lambda^2)^{1/2} \left[\left(\frac{x}{x_0} \right)^2 \left(\frac{x_0^{1-\lambda} - \kappa x_0^{1+\lambda}}{x_0^{1-\lambda} - \kappa x^{1+\lambda}} \right)^2 - 1 \right]^{-1/2} \frac{dx}{x}$$

$$+2 \int_{x_b}^{\infty} \left(\frac{1}{1 - \frac{1}{x}} \right)^{1/2} \left[\left(\frac{x}{x_0} \right)^2 \frac{a^2(x_0^{1-\lambda} - \kappa x_0^{1+\lambda})^2}{1 - \frac{1}{x}} - 1 \right]^{-1/2} \frac{dx}{x} - \pi \quad (23)$$

and

$$\sin \theta = \frac{2M}{D_d} \frac{x_0}{a(x_0^{1-\lambda} - \kappa x_0^{1+\lambda})} \quad (24)$$

where a and κ are given by 19

It was shown in [21] that in JMN metric the parameter range when there is relativistic deflection is given as $M_0 > 0.475$. Indeed for $M_0 > 2/3$ there is photon sphere and deflection angle becomes infinite. In Tolman-VI solution however there is no photon sphere. But it turns out that the maximal deflection becomes $> 2\pi$ for $\lambda \lesssim 0.44$ or equivalently $x_b < 2.25$

The relativistic images for metric having a photon sphere are clumped together around the angular location of photon sphere and successive images are exponentially demagnified [32]. This holds true for both Schwarzschild and JNW metric (in appropriate parameter range where there is a photon sphere). So there is a forbidden angular region in which no images can form and the critical angle corresponds to the angular location of photon sphere. This is true only if there is a single (unstable) photon sphere in the spacetime. For multiple photon spheres one can have additional images corresponding to light rays that go inside the outer photon sphere and turn back and so the lensing signature is expected to be qualitatively different. While this is interesting avenue for further study, we do not consider such cases in this paper.

In the absence of photon sphere, for example in the JMN metric when $M_0 < 2/3$, the images are better separated and although highly demagnified, the magnification is of the same order of magnitude for successive images as demonstrated in [21]. We simply note here that both these features qualitatively generalize for the Tolman-VI metric despite quantitative differences and the numbers involved are in the same ballpark. As it is not very enlightening, we forgo the presentation of image positions and magnifications for Tolman-VI metric. Also as with the JMN metric the deflection angle monotonically increases with decreasing impact parameter and consequently for reasons presented in [21] there are no radial critical curves in Tolman-VI solution.

VI. EINSTEIN RING

If the source, the lens, and the observer lie on a single straight line, i.e., in the so-called aligned configuration, a circular image pattern known as the Einstein Ring (ER), is formed. The rings formed by photons which have been deflected by $2\pi, 4\pi$ etc are referred to as relativistic rings. For

Schwarzschild and weakly naked JNW cases, there are in principle infinite number of relativistic ERs and they are located very close to angular location of photon sphere. This is called the critical angle θ_{crit} , and angular location of all images has to be greater than θ_{crit} . For a Schwarzschild black hole $4 \times 10^6 M_\odot$ at 8.5 kpc one gets $\theta_{crit} \sim 24.1$ microarcseconds and for $100 M_\odot$ at 1 kpc one gets $\theta_{crit} \sim 5.1$ nanoarcseconds. In contrast, for SNS, ER and images are formed below the critical angle for corresponding Schwarzschild black hole, and are reasonably well separated. In table I and II, we show angular location of Relativistic ER for $4 \times 10^6 M_\odot$ at 8.5 kpc and for $100 M_\odot$ at 1 kpc respectively for both SNS metrics studied in the paper.

TABLE I: Angular location of relativistic ER for $4 \times 10^6 M_\odot$ at 8.5 kpc for both SNS metrics studied in the paper: θ is in microarcseconds

ER	JMN($M_0 = 0.63$)	JMN($M_0 = 0.615$)	Tolman-VI ($\lambda = 0.13$)	Tolman-VI ($\lambda = 0.14$)
I	23.96	23.38	14.90	14.83
II	20.76	16.50	7.87	7.59
III	15.26	5.96	4.33	3.89
IV	8.17	*	1.90	*

TABLE II: Angular location of Relativistic ER for $100 M_\odot$ at 1 kpc for both SNS metrics studied in the paper: θ is in nanoarcseconds

ER	JMN($M_0 = 0.63$)	JMN($M_0 = 0.615$)	Tolman-VI ($\lambda = 0.13$)	Tolman-VI ($\lambda = 0.14$)
I	5.09	4.96	3.16	3.15
II	4.41	3.51	1.67	1.61
III	3.24	1.26	0.92	0.82
IV	1.73	*	0.40	*

In next section we compute and analyze the time delay between relativistic ERs for these spacetimes.

VII. TIME DELAY

Coordinate time taken by photon to travel from r_0 to r is given by

$$t(r, r_0) = \int_{r_0}^r \sqrt{\frac{1}{f(r)g(r)}} \frac{1}{\sqrt{1 - \frac{h(r_0)r_0^2}{h(r)r^2} \frac{g(r)}{g(r_0)}}} dr \quad (25)$$

Let \mathcal{R}_s and \mathcal{R}_o be, the radial coordinates of the source and the observer measured from the center of lens. In dimensionless units they are given as

$$\chi_s = \frac{\mathcal{R}_s}{2M} \text{ and } \chi_o = \frac{\mathcal{R}_o}{2M}. \quad (26)$$

From geometry of the configuration we can write χ_s and χ_o in terms of distances and angles involved as [19]

$$\begin{aligned} \chi_s &= \frac{D_s}{2M} \sqrt{\left(\frac{D_{ds}}{D_s}\right)^2 + \tan^2 \beta}, \\ \chi_o &= \frac{D_d}{2M}, \end{aligned} \quad (27)$$

As we are concerned with ER only, we take $\beta = 0$. Then as we take $\frac{D_{ds}}{D_s} = \frac{1}{2}$, we have $\chi_s = \chi_o$ and equivalently $\mathcal{R}_o = \mathcal{R}_s$. Now time difference between m th and n th relativistic ER is given by

$$\Delta t_{m,n} = 2t(\mathcal{R}_0, r_{0_m}) - 2t(\mathcal{R}_0, r_{0_n}) \quad (28)$$

where r_{0_m} is the distance of closest approach corresponding to m th relativistic ER. Scaling by Schwarzschild time and writing in dimensionless units $\tau = \frac{t}{2M}$ and for notational simplicity writing $\tau(\chi_o, x_0)$ as $\tau(x_0)$ we list below the time delay formulae for cases under study.

SpaceTime	Time Delay Formulae (Dimensionless)
Schwarzschild	$\tau(x_0) = 2 \int_{x_0}^{\chi_o} \frac{1}{1-\frac{1}{x}} \frac{1}{\sqrt{1-\frac{x_0^2}{x^2} \frac{(1-\frac{1}{x})}{(1-\frac{1}{x_0})}}} dx$
JMN	$\tau(x_0) = 2 \int_{x_0}^{x_b} \frac{1}{\sqrt{(1-M_0^2)(xM_0)^\gamma}} \frac{1}{\sqrt{1-\frac{x_0^2}{x^2} \frac{x^\gamma}{x_0^\gamma}}} dx + 2 \int_{x_b}^{\chi_o} \frac{1}{1-\frac{1}{x}} \frac{1}{\sqrt{1-\frac{x_0^2}{x^2} \frac{(1-\frac{1}{x})}{(1-M_0)(x_0M)^\gamma}}} dx$
Tolman-VI	$\tau(x_0) = 2 \int_{x_0}^{x_b} \frac{1}{\sqrt{(1-M_0^2)(xM_0)^\gamma}} \frac{1}{\sqrt{1-\frac{x_0^2}{x^2} \frac{x^\gamma}{x_0^\gamma}}} dx + 2 \int_{x_b}^{\chi_o} \frac{1}{1-\frac{1}{x}} \frac{1}{\sqrt{1-\frac{x_0^2}{x^2} \frac{(1-\frac{1}{x})}{(1-M_0)(x_0M)^\gamma}}} dx$
JNW	$\tau(x_0) = 2 \int_{x_0}^{\chi_o} \frac{1}{(1-\frac{1}{\nu x})^\nu} \frac{1}{\sqrt{1-\frac{x_0^2}{x^2} \frac{(1-\frac{1}{\nu x})}{(1-\frac{1}{\nu x_0})}}} dx$

The time delay in terms Schwarzschild time is given as

$$\Delta \tau_{m,n} = \tau(x_{0_m}) - \tau(x_{0_n})$$

Below we highlight the qualitative differences in the behavior of relativistic time delay for spactimes with a photon sphere from those without one.

A. Singularities with a photon sphere (Black Holes and WNS)

As has been discussed earlier if the spacetime has a photon sphere then there is a forbidden angular region and all relativistic images are located close to each other and near the angular

location of photon sphere. In this case the time delay between successive relativistic rings is more or less constant and is neatly related to light travel time in a circle on photon sphere. This is intuitive to understand because in presence of photon sphere the light trajectories corresponding to successive rings differ by one extra nearly circular loop at photon sphere radius as can be easily seen from figure 2. Indeed the time delay between ERs is well approximated by

$$\Delta t_{m,n} = \frac{2\pi(m-n)r_{ph}}{\sqrt{g(r_{ph})}} = 2\pi(m-n)J_{ph} \quad (29)$$

where r_{ph} is radius of photon sphere and J_{ph} is corresponding impact parameter [36]. For Schwarzschild black hole time delay between successive relativistic ER then becomes roughly $2\pi \times 3\sqrt{3}M$ and for JNW it becomes $2\pi \times \frac{1+2\nu}{\nu} \left(1 - \frac{2}{1+2\nu}\right)^{\frac{1-2\nu}{2}} M$. For same Schwarzschild mass, increasing scalar charge decreases the time delay. Thus as with the case for position and magnification of relativistic images in the presence of photon sphere, the time delay is also determined by the metric near photon sphere and displays certain universal features irrespective of presence or absence of event horizon. Also as far as observations are concerned, since in such a situation, higher order relativistic images are clumped together (and excessively demagnified) [32], the relevant observational quantity should be time delay between first and second images. The scenario becomes different in absence of photon sphere as we discuss below.

B. Singularities without photon sphere (SNS)

TABLE III: Time delay for $4 \times 10^6 M_\odot$ at 8.5 kpc for both SNS metrics studied in the paper: $\Delta\tau$ is in second

Time Delay	JMN($M_0 = 0.63$)	JMN($M_0 = 0.615$)	Tolman-VI ($\lambda = 0.13$)	Tolman-VI ($\lambda = 0.14$)
$\Delta\tau_{2,1}$	299.6	272.0	145.8	141.9
$\Delta\tau_{3,2}$	242.4	151.8	78.8	74.9
$\Delta\tau_{4,3}$	157.7	*	41.4	*

TABLE IV: Time delay for $100M_\odot$ at 1 kpc for both SNS metrics studied in the paper: $\Delta\tau$ is in milisecond

Time Delay	JMN($M_0 = 0.63$)	JMN($M_0 = 0.615$)	Tolman-VI ($\lambda = 0.13$)	Tolman-VI ($\lambda = 0.14$)
$\Delta\tau_{2,1}$	7.5	6.8	3.6	3.5
$\Delta\tau_{3,2}$	6.1	3.8	2.0	1.9
$\Delta\tau_{4,3}$	3.9	*	1.0	*

In the absence of photon sphere the time delay between successive images is no longer roughly constant. Explicit calculation for various cases shows that the successive time delays go on decreasing. In table III and IV, we show time delay between Relativistic ER for $4 \times 10^6 M_\odot$ at 8.5

kpc and for $100M_{\odot}$ at 1 kpc respectively for both SNS metrics studied in the paper. It remains to be seen if this is a feature generic to SNS with monotonic deflection angle. In passing we note that for the particular cases we have studied here, the successive time delay are lesser for Tolman-VI case as compared to the corresponding JMN case, where by corresponding we mean spacetimes admitting same maximal deflection and hence same number of relativistic images and rings. and also the time delay is lesser in general than a black hole with corresponding Schwarzschild mass. In case the images are expected to be resolved (like the super massive black hole case) the time delay between first and last images also becomes an observational quantity of interest. One can expect that to be fairly large if there are large number of images as successive time delay will add up. But the decreasing trend in successive time delay compensates for this phenomenon to some extent. For super massive black hole case the time delay is of order of seconds. For $100M_{\odot}$ objects at kpc distances, the time delay becomes of the order of milliseconds. In this case images are also unlikely to be resolved (separation as discussed earlier being of the order of nanoarcseconds). But if there is a characteristic variability of source one might hope to find signatures in the unresolved image. Relativistic Microlensing studies in such cases might be interesting idea to pursue.

VIII. DISCUSSION AND CONCLUSION

In this paper, we have studied the time delay properties of gravitational lenses in strong deflection regime when relativistic images can be formed, and its role as an in principle probe of the cosmic censorship question. Three of the four metric we have considered in this paper have been previously explored from relativistic lensing perspective. For the fourth one viz Tolman-VI solution we find that the basic features for image positions and magnification is similar to JMN case without photon sphere. Thus the lensing signatures for the JMN case, which happens to be a toy example of naked singularity solution obtained as collapse end state for a fluid with zero radial pressure, qualitatively generalize for analogous scenario with inclusion of radial pressure i.e. the Tolman-VI case. We have also presented in this paper the time delay between relativistic ER for both JMN and Tolman-VI cases both of which serve as examples of SNS and contrasted them with previously studied examples for relativistic time delay in literature which, to the best of our knowledge, have all been either black holes or WNS [6, 27, 37]. We have confirmed/shown that there are important differences between SNS and WNS for time delays between relativistic images which we discuss below.

We have used the Schwarzschild black hole, which has a photon sphere at Schwarzschild radius

of $3M$ as a standard, against which the time delay difference between successive Einstein Rings for our cases of interest are compared. For the differential time delay between relativistic images formed by successive loops made by photon, there is practically no difference between sources along the optic axis and slightly misaligned ones. Moreover only strongly aligned configurations are of importance for lensing. Hence, in this work we have presented the relativistic time delay only between the successive Einstein Rings. This time delay is of order of few seconds for the galactic center super massive object where as it is of the order of milliseconds for 100 solar mass objects in our galaxy at kpc distance scales.

For the Schwarzschild black holes, the time delay difference is very close to $2\pi \times 3\sqrt{3}M$, which is 2π times the critical impact parameter as to be expected. Other spacetimes with photon sphere will emulate this feature though the time delay difference will be different as it will depend on other parameters that characterize the spacetime apart from mass. As an example, consider the JNW metric discussed in section VII A where this time delay difference decreases with increasing scalar charge. The contrasting scenario is the case of formation of multiple relativistic Einstein rings in the presence of naked singularities not covered by photon sphere. Then, the successive Einstein rings formed for a source close to the optic axis of the lens will have successively smaller impact parameters. The differential time delay between these rings will progressively decrease as was shown in section VII B for two prototype examples. If we were to detect time delay of this nature, possibly we have a scenario where the cosmic censorship is violated. This requires the images to be resolved. However, even when the images are not resolved, one can possibly discriminate SNS from WNS and black holes. This is because an intrinsic source variability will show up almost periodic, but, less luminous change in the flux in the unresolved composite Einstein Rings for black holes and WNS where as there would be no such periodicity for SNS. Thus there are important differences in ratio of time delays between successive relativistic images for spacetimes with photon sphere and those without photon sphere and this might be helpful in observationally distinguishing SNS from WNS and black holes. As we have remarked earlier, we have not considered multiple photon sphere spacetimes in this study and WNS with multiple photon sphere will have signature different from WNS studied in this paper.

Observation of relativistic images will be a wonderful test of gravitational physics in strong field regime. Practical difficulties and technological challenges notwithstanding, VLBI is a promising technique which might in near future achieve angular and time resolution to bring at least some of the questions that relativistic lensing can probe such as the one that we studied here under observational purview, at least for the galactic central super massive object [38, 39]. With this

in mind it will be useful to study more realistic examples of naked singularities and under more realistic astrophysical conditions.

Acknowledgments

We would like to thank Dr. K.S.Virbhadra for valuable correspondence and the anonymous Referee for valuable comments and suggestions.

-
- [1] C. Darwin, Royal Society of London Proceedings Series A **249**, 180 (1959).
 - [2] C. Darwin, Royal Society of London Proceedings Series A **263**, 39 (1961).
 - [3] G. Campbell and R. Matzner, J.Math.Phys. **14**, 1 (1973).
 - [4] C. T. Cunningham and J. M. Bardeen, Astrophysics J. Lett. **173**, L137 (1972).
 - [5] C. T. Cunningham and J. M. Bardeen, Astrophys. J. **183**, 237 (1973).
 - [6] K. S. Virbhadra and G. F. R. Ellis, Phys. Rev. D **62**, 084003 (2000).
 - [7] K. S. Virbhadra and G. F. R. Ellis, Phys.Rev. **D65**, 103004 (2002).
 - [8] R. Penrose, Nuovo Cimento Rivista Serie **1**, 252 (1969).
 - [9] K. Nomoto, Proceedings of the International Astronomical Union **7**, 1 (2011), ISSN 1743-9221.
 - [10] P. S. Joshi, *Gravitational Collapse and Spacetime Singularities* (Cambridge University Press, 2007).
 - [11] P. S. Joshi and D. Malafarina, International Journal of Modern Physics D **20**, 2641 (2011), 1201.3660.
 - [12] T. Harada, Pramana **63**, 741 (2004), gr-qc/0407109.
 - [13] T. Harada and H. Maeda, Phys.Rev. **D63**, 084022 (2001), gr-qc/0101064.
 - [14] A. Ori and T. Piran, Phys.Rev.Lett. **59**, 2137 (1987).
 - [15] A. Ori and T. Piran, Phys.Rev. **D42**, 1068 (1990).
 - [16] P. S. Joshi, D. Malafarina, and R. V. Saraykar, Int.J.Mod.Phys. **D21**, 1250066 (2012), 1107.3749.
 - [17] M. Visser, C. Barcelo, S. Liberati, and S. Sonego (2009), 0902.0346.
 - [18] K. Virbhadra, D. Narasimha, and S. Chitre, Astron.Astrophys. **337**, 1 (1998), astro-ph/9801174.
 - [19] K. S. Virbhadra and C. R. Keeton, Phys.Rev. **D77**, 124014 (2008), 0710.2333.
 - [20] G. N. Gyulchev and S. S. Yazadjiev, Phys.Rev. **D78**, 083004 (2008), 0806.3289.
 - [21] S. Sahu, M. Patil, D. Narasimha, and P. S. Joshi, Phys.Rev. **D86**, 063010 (2012), 1206.3077.
 - [22] Z. Kovacs and T. Harko, Phys.Rev. **D82**, 124047 (2010), 1011.4127.
 - [23] P. S. Joshi, D. Malafarina, and R. Narayan (2013), 1304.7331.
 - [24] S. Refsdal, Mon.Not.Roy.Astron.Soc. **128**, 307 (1964).
 - [25] R. Blandford and R. Narayan, Ann.Rev.Astron.Astrophys. **30**, 311 (1992).
 - [26] D. Narasimha, Bulletin of the Astronomical Society of India **30**, 723 (2002).
 - [27] V. Bozza and L. Mancini, Gen.Rel.Grav. **36**, 435 (2004), gr-qc/0305007.

- [28] P. S. Joshi, D. Malafarina, and R. Narayan, *Class.Quant.Grav.* **28**, 235018 (2011), 1106.5438.
- [29] R. Genzel, F. Eisenhauer, and S. Gillessen, *Reviews of Modern Physics* **82**, 3121 (2010), 1006.0064.
- [30] V. Bozza, *Phys.Rev.* **D78**, 103005 (2008), 0807.3872.
- [31] R. C. Tolman, *Phys.Rev.* **55**, 364 (1939).
- [32] V. Bozza, *Phys.Rev.* **D66**, 103001 (2002), gr-qc/0208075.
- [33] C.-M. Claudel, K. Virbhadra, and G. Ellis, *J.Math.Phys.* **42**, 818 (2001), gr-qc/0005050.
- [34] W. Hasse and V. Perlick, *Gen.Rel.Grav.* **34**, 415 (2002), gr-qc/0108002.
- [35] M. Karlovini, K. Rosquist, and L. Samuelsson, *Mod.Phys.Lett.* **A17**, 197 (2002), gr-qc/0009073.
- [36] V. Bozza and L. Mancini, *Gen.Rel.Grav.* **36**, 435 (2004), gr-qc/0305007.
- [37] E. A. Larranaga Rubio (2003), gr-qc/0309108.
- [38] J. S. Ulvestad, *New Astron.Rev.* **43**, 531 (1999), astro-ph/9901374.
- [39] V. L. Fish and S. S. Doeleman, *IAU Symp.* **261**, 271 (2009), 0906.4040.